Journal of Oceanography, Vol. 62, pp. 321 to 330, 2006

Features of Ocean Microwave Emission Changed by Wind at 6 GHz

AKIRA SHIBATA*

Earth Observation Research and application Center (EORC), Japan Aerospace Exploration Agency (JAXA), Harumi, Chuo-ku, Tokyo 104-6023, Japan

(Received 20 May 2005; in revised form 12 December 2005; accepted 13 December 2005)

Ocean microwave emissions changed by the ocean wind at 6 GHz were investigated by combining data of the Advanced Microwave Scanning Radiometer (AMSR) and SeaWinds, both aboard the Advanced Earth Observation Satellite-II (ADEOS-II). This study was undertaken to improve the accuracy of the sea surface temperature (SST) retrieved from the AMSR 6 GHz data. Two quantities, 6V*(H*), were defined by the brightness temperature of the AMSR at 6 GHz with two polarizations (V-pol and H-pol), adjusted for atmospheric effects and with a calm ocean surface emission removed. These quantities represent a microwave emission change due to the ocean wind at 6 GHz. 6V* does not change in a region where 6H* is less than around 4 K (referred to as z0). Both 6V* and 6H* increase above z0. The 6V* to 6H* ratio, sp, varies with the relative wind directions. Furthermore, the sp values vary with the SST, between the northern and southern hemisphere, and seasonally. By specifying appropriate values for z0 and sp, the SST error between AMSR and buoy measurement became flat against 6H*, which is related to the ocean wind. Two extreme cases were observed: the Arabian Sea in summer and the Northwestern Atlantic Ocean in winter. The air-sea temperature difference in the former case was largely positive, while it was largely negative in the latter. The 6V* and 6H* relations differed from global conditions in both cases, which resulted in incorrect SSTs in both areas when global coefficients were applied.

Keywords:
· Microwave radiometers,
· sea surface temperature,
· AMSR,
· SeaWinds,
· rms error 0.59°C.

1. Introduction

Passive microwave radiometers observe the microwave emission from the Earth at several frequencies. Two almost identical microwave radiometers were launched in 2002, the Advanced Microwave Scanning Radiometer for Earth Observing System (AMSR-E) on AQUA, launched by the National Aeronautics and Space Administration (NASA) on May 4, 2002, and the AMSR on the Advanced Earth Observing Satellite-II (ADEOS-II), launched by the Japan Aerospace Exploration Agency (JAXA) on Dec. 14, 2002. The AMSR and AMSR-E units (hereafter AMSRs) were made by JAXA (Kawanishi *et al*., 2003). AMSRs use several frequencies from 6 GHz to 89 GHz.

The sea surface temperature (SST) can be retrieved by combining data at several frequencies from AMSRs (Shibata, 2004). The best frequencies for measuring the SST lie between 4 and 10 GHz (Hollinger and Lo, 1984). The microwave SST may be retrieved through clouds, while the infrared SST cannot.

In algorithms for retrieving SST by passive microwave radiometers, wind effects on ocean microwave emissions are the greatest and most difficult error to eliminate (Shibata, 2004). To accurately retrieve the SST, we should determine the features of ocean microwave emission at 6 GHz, responding to the ocean wind. The ocean wind varies rapidly both spatially and temporally, and it is difficult to observe accurately. A NASA scatterometer, SeaWinds, was installed on ADEOS-II. SeaWinds is an active sensor operated at 13.4 GHz. One primary purpose of SeaWinds was to measure ocean wind vectors (Liu, 2002). As a result, we can estimate the features of ocean microwave emission at 6 GHz related to the ocean wind by combining data of the AMSR and SeaWinds on ADEOS-II.

This paper presents descriptions of the sensors and AMSRs' SST algorithm, descriptions of ocean microwave emissions changed by the ocean wind at 6 GHz, as de-

* E-mail address: shibata.akira@jaxa.jp

rived from the global ocean and from the Arabian Sea in summer and the Western Atlantic Ocean in winter. Finally, a discussion of the results and conclusions are presented.

2. Sensors

AMSRs are forward-looking, conically scanning radiometers positioned at a constant-incidence angle of 55 degrees (Kawanishi *et al.*, 2003). Photo. 1 shows an exterior view of the AMSR-E sensor unit during a final test before attachment to the AQUA satellite. The diameter of the main antenna is 2 m for AMSR, and 1.6 m for AMSR-E. The main antenna rotates at 40 rpm for both AMSRs. Table 1 shows frequencies and polarizations of AMSRs. The spatial resolution on the Earth's surface at 6 GHz is 40 × 70 km for AMSR, and 43 × 75 km for AMSR-E. The spatial sampling interval on the Earth's surface is 10 km at all frequencies except for 89 GHz, at which it is 5 km. The temperature resolution at 6 GHz is 0.34 K for both AMSRs.

The SeaWinds emits the microwave radiation and measures the microwave echo from the Earth's surface. The ocean wind speed and direction can be retrieved from the SeaWinds data (Liu, 2002). We used the Level 2B geophysical data of SeaWinds with spatial resolution 25 km. Unfortunately, ADEOS-II stopped operating on October 25, 2003, due to a failure of an electronic cable from a solar panel. The period of SeaWinds L2 data available was from April 11 to October 24.

3. SST Algorithm

The best frequencies for measuring the SST lie between 4 and 10 GHz (Hollinger and Lo, 1984). The sensitivity of the ocean microwave emission to the SST varies with frequencies and SST. The sensitivity at V-pol is larger than that at H-pol. For examples, the sensitivity at 4 GHz V-pol is 0.44 K/°C at SST 0°C, and 0.49 K/°C at 30°C. At 10 GHz V-pol (10V), it is 0.08 K/°C and 0.58 K/°C, respectively. We base our SST algorithm on the 6V brightness temperature (Tb). Figure 1 depicts the relation between the ocean surface Tb of 6V(H) and the SST. The relation was obtained using the Fresnel formula, with an incidence angle of 55.0 degrees and a salinity of 35 PSU. The complex dielectric constant of the ocean water was obtained from Klein and Swift (1977).

Figure 1 was computed for calm ocean conditions, and without atmospheric effects. AMSR 6V contains both effects. For accurate SST estimations, we should make these two corrections ((a) wind correction and (b) atmospheric correction) for the AMSR 6V. Furthermore, we should make (c) salinity correction, and (d) incidence angle correction. Finally, we should remove contamination by several sources: (e) removal of the land contamination area, (f) removal of the sea ice contamination area,

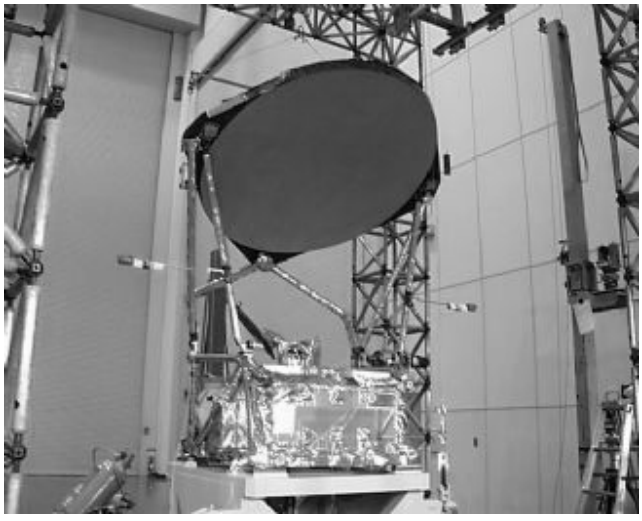

Photo. 1. Exterior view of AMSR-E.

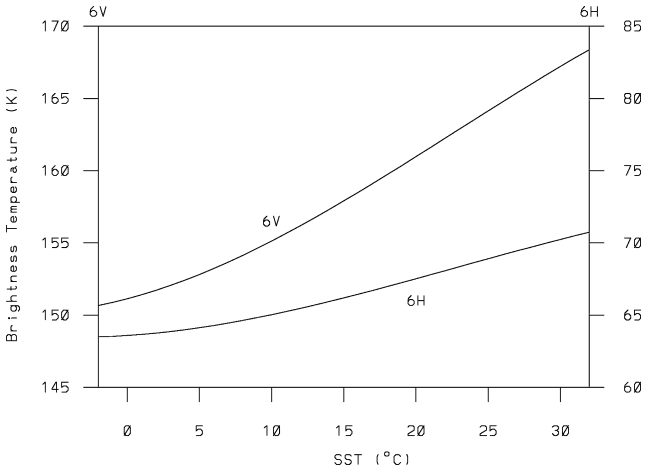

Fig. 1. Relation between 6V(H) and SST.

Table 1. Frequencies (GHz) and polarizations of AMSRs.

AMSR	6.925 V/H	10.65 V/H	18.7 V/H	23.8 V/H	36.5 V/H	50.3 V	52.3 V	89.0 V/H
AMSR-E	same	same	same	same	same	—	—	same

(g) removal of the sun glitter contamination area, and (h) removal of the radio frequency interference (RFI) contamination area.

A method of correcting the wind effect will be explained in detail in Section 4. The maximum range of wind correction was 6 K. The atmospheric correction was calculated from a simulation of Tb using a microwave-transferring model (Shibata, 2004). The simulated Tb was calculated for 6V, 6H, 23V, and 36V under various atmospheric vertical conditions, with constant SST from 0 to 35°C SST at intervals of 5°C. From these data sets, the Tb of 6V(H) was averaged at two-dimensional grids of 23V and 36V, both of whose grid intervals are 1 K. So we have the averaged 6V(H), defined as simu_6V(H), at grids of 23V and 36V at constant SST. The atmospheric effect, atmos_effect_6V(H), was defined by Eq. (1).

$$\text{atmos\_effect\_6V(H)} = \text{simu\_6V(H)} - \text{calm\_ocean\_6V(H)}, \quad (1)$$

where calm_ocean_6V(H) is given by the relations in Fig. 1. The value of atmos_effect_6V(H) is given by specifying the values of SST, 23V and 36V. In rainy conditions, the microwave energy at 36 and 23 GHz is scattered by raindrops, and we are unable to use those data quantitatively. In our algorithm, the SST is set as missing under rainy conditions. The maximum range of atmospheric correction on 6V was 2 K.

The sensitivity to salinity at 6V is 0.005 K/PSU at 0°C SST, and –0.0071 K/PSU at 30°C SST, when the salinity changes from 30 to 35 PSU. In the SST algorithm, we corrected the salinity effect by using the monthly climate salinity. The incidence angle correction was less than 0.3 K.

We need an initial SST value as one of the inputs in our SST algorithm. As we shall see in Section 4, the wind effect is estimated using 6H. The dependence of 6H on the SST is comparatively smaller than that of 6V, as shown in Fig. 1, but it cannot be neglected. We use the initial SST to remove the dependence of 6H on the SST. We also use the SST to calculate the atmospheric effect defined by Eq. (1). We can specify this initial SST by one of two methods, climate SST or Reynolds SST. The climate SST is a monthly average over the past 30 years, the Reynolds SST is a weekly analysis (Reynolds and Smith, 1994). We typically use the latter. We estimate the AMSRs' SST error due to an initial SST error in Section 4.

After we made the four corrections (a) to (d) on the AMSRs 6V, we applied the relation of 6V and SST in Fig. 1 to retrieve the SST. We made some small adjustments to the theoretical values for 6V since the complex dielectric constant may be not quite perfect. These adjustments became more substantial for lower SST values. The values for adjustments were specified with a 10°C interval, and interpolated for the intermediate SSTs: e.g., –0.5 K at SST 0°C and 0.0 K at SST 30°C. These adjustments were based on results from SST comparisons between AMSRs and buoy data.

4. Microwave Emission Change at 6 GHz in the Global Ocean

To investigate the features of ocean microwave emission changed by ocean wind at 6 GHz, we combined data

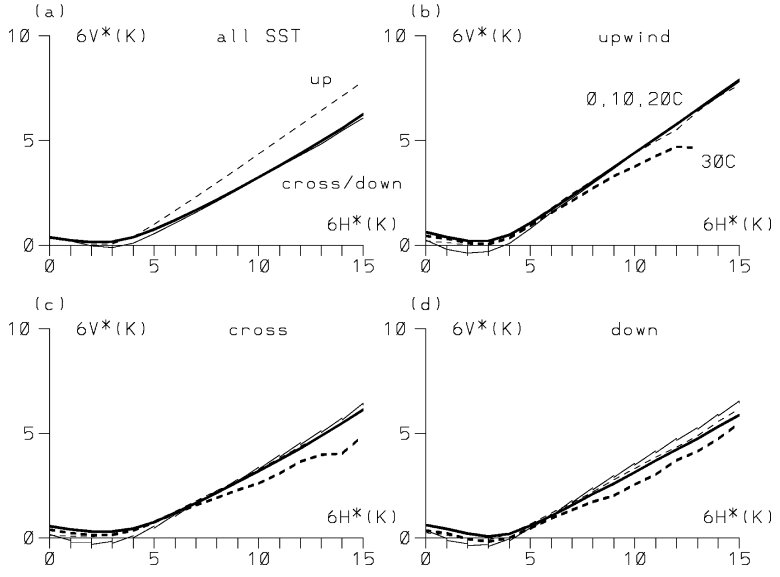

Fig. 2. Relations of 6V* and 6H* (K) in the global ocean in July 2003. (a) relations averaged among three relative wind directions, (b) upwind direction with four SST ranges overlapped, (c) crosswind direction, and (d) downwind direction.

of AMSR and SeaWinds on ADEOS-II. The spatial sampling of AMSR is 10 km; however, the spatial resolution at 6 GHz is on the order of 50 km. We sampled the AMSR data with a 30 km interval, and averaged the SeaWinds data within 50 km of the AMSR resolution. Figure 2 shows the results in July 2003 in the global ocean. The values of 6V* and 6H* in Fig. 2 are obtained by Eq. (2).

$$6V(H)^* = \mathrm{AMSR\_6V(H)} - \mathrm{atmos\_effect\_6V(H)} - \mathrm{calm\_ocean\_6V(H)}, \quad (2)$$

where AMSR_6V(H) is AMSR Tb at 6 GHz; atmos_effect_6V(H) and calm_ocean_6V(H) are the same as in Eq. (1). We averaged 6V* with the 1 K interval of 6H*, and plotted the data in cases for sample numbers exceeding 10. Total sample numbers were 6 million, and the sample numbers of each point range from 10 to 300,000. In accordance with higher SST and larger 6H*, the sample number decreased rapidly. 6V(H)* represent the quantity of ocean microwave emission changed by ocean wind at 6 GHz.

Three relative wind directions are depicted in Fig. 2(a). The relative wind direction is defined as the relative angle between the AMSR viewing direction and the SeaWinds wind direction. Relative angles between 0 and 20 (or between 340 and 360) degrees correspond to an upwind direction (indicated by the broken line); angles between 80 and 100 (or between 260 and 280) correspond to a crosswind (the bold line); angles between 160 and 200 correspond to a downwind (the thin line). Figure 2(a) indicates that 6V* does not change in a region where 6H* is less than around 4 K (referred to as z0) and that both 6V* and 6H* increase above z0. The slope of 6V*/6H* increase (designated as sp) varied among the three relative wind directions. The sp value for upwind was the greatest, while the values for the other two directions were smaller, and almost the same. Even though values of z0 appear to differ slightly among the three relative wind directions, z0 was set as 3.8 K in AMSRs' SST algorithm for simplicity.

Figures 2(b)–(d) compares the sp values in the four SST ranges. Figure 2(b) corresponds to the upwind, Fig. 2(c) to crosswind, and Fig. 2(d) to downwind direction, in which the four SST ranges are overlapped, respectively. The four SST ranges correspond to SST0°C (SST< 2.5°C, indicated by the thin line), SST10°C (7.5 < SST < 12.5°C, the bold line), SST20°C (17.5 < SST < 22.5°C, the dotted thin line), and SST30°C (27.5°C < SST, the dotted bold line). The sp values of SST30°C were slightly smaller than those of other SSTs for three relative directions.

The relations between 6V(H)* and the SeaWinds wind speed are shown in Fig. 3 (upper: 6V*, lower: 6H*). We showed 6V(H)* only in crosswind condition, and with four SST ranges overlapping in July 2003. 6H* appear to

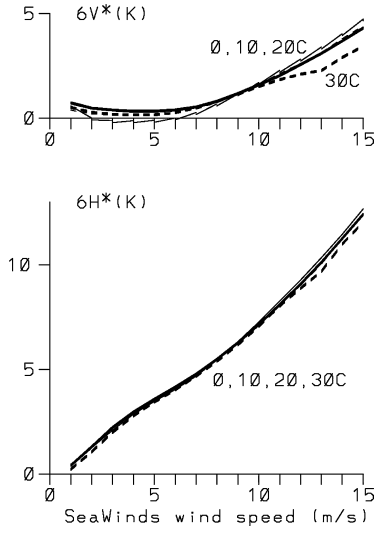

Fig. 3. Relations of 6V* and 6H* to SeaWinds wind speed for four SST ranges in July 2003.

be almost the same for all SST ranges. 6V* is almost the same except for SST30°C, while 6V* at SST30°C differs from the other SST ranges. This result indicates that the different sp at SST30°C in Fig. 2(c) is due to 6V*, not to 6H*. We discuss likely causes of these results in Section 6.

The relations of 6V* and 6H* shown in Fig. 2 were derived from the global data, i.e., averaging data in the northern hemisphere (NH) and southern hemisphere (SH). In fact, the relation appeared to differ slightly between the NH and SH. The difference between the NH and SH around SST10°C was comparatively greater among four SST ranges. Figure 4 illustrates the sequential change of 6V(H)* in four months (Apr., Jun., Jul., and Oct. 2003) in the SST10°C. The thin line in Fig. 4 corresponds to the SH and the solid line to the NH. All data represent only crosswind conditions. The relations were almost the same between the NH and SH in the two months of Apr. and Oct. The sp value in the NH was smaller than that in the SH in the two months of Jun. and Jul. These results indicate that the sp should be changed not only with the SST but also seasonally and locally (NH or SH).

We can calculate a wind correction on 6V (designated as inc_6V) by Eq. (3).

$$\begin{aligned} \mathrm{inc\_6V} &= 0 && \text{for 6H* less than z0,} \\ &= (6H^* - z0) \times sp && \text{for 6H* greater than z0.} \end{aligned} \quad (3)$$

The values of sp depend on the relative wind direction, and the average value among three relative winds is 0.5 from Fig. 2(a). We count the SST as missing when 6H* exceeds (z0 + 9) to avoid SST errors under very high wind

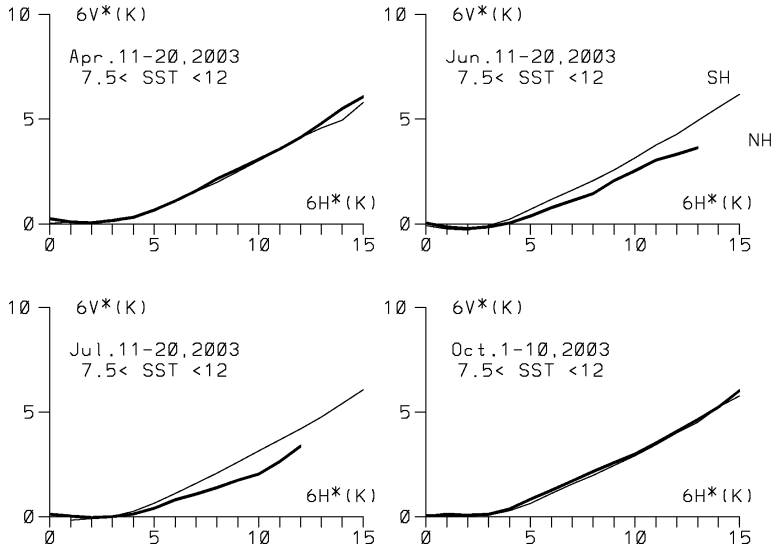

Fig. 4. Comparison of 6V* and 6H* relations between NH (solid) and SH (thin) averaged during 10 days on each month of Apr., Jun., Jul., Oct. 2003.

speeds. The relations of 6V* and 6H* shown in Fig. 2(a) appear linear even for a greater 6H*. But these relations were obtained from the global data. As we see in the extreme cases in Section 5, values of z0 and sp may differ depending on various atmospheric and oceanic conditions. To avoid SST errors under such extreme cases, we count the SST as missing for the greater 6H*.

In our SST algorithm, we need the SST for one of the initial inputs; the SST was used to calculate calm_ocean_6H and 6H* in Eq. (2). As seen in Fig. 1, the sensitivity at 6H to the SST is 0.25 K/°C on average. If there is a 1°C error in the initial SST, it corresponds to a 0.25 K error of 6H*. When 6H* is less than z0, there is no error in inc_6V, as seen in Eq. (3). When 6H* is greater than z0, the error of inc_6V is 0.125 K, which corresponds to a 0.25°C error of the SST.

In applying Eq. (3) to the wind correction, we must know the relative wind direction. We can estimate the relative wind direction using AMSR's data. As illustrated in Fig. 2(a), 6V(H)* values have an anisotropic feature depending on the relative wind directions. The anisotropic feature was first reported from 37 GHz data of the Special Sensor Microwave/Imager (SSMI) (Wentz, 1992). The anisotropic feature becomes more significant with higher frequencies, i.e., that at AMSRs 36 GHz is more significant than 6 GHz. We used a two-dimensional plane of 6H* and a quantity (s36) derived from AMSRs 36 GHz (Shibata, 2004). In this plane, positions of (6H*, s36) are separated in accordance with three relative wind directions. We can determine the relative wind direction from these positions.

Both seasonal and spatially changes of sp values are accommodated in the SST algorithm (version 2) adopted by the JAXA. To evaluate the accuracy of AMSR's SST, we calculated the rms of SST difference between AMSRs and buoy data. The buoy data were collected through the Global Telecommunications System (GTS) and included data from both moored and drifting buoys. We averaged the AMSRs SST within each 3×3 sample area. The temperature resolution of AMSRs 6 GHz is 0.34 K per sample, which corresponds to 0.7°C SST error. By averaging the 3×3 samples, the error should be reduced to 1/3. We omitted cases in which the difference between maximum and minimum AMSRs SST was larger than 3°C within the 3×3 samples. We also omitted cases where the absolute difference between the AMSRs and buoy SST was larger than 4°C. The difference of observation time between AMSRs and buoy was less than 1 hour. The rms of the SST difference was 0.59°C for AMSR-E over 12 months from January to December 2003, and 0.69°C for AMSR over seven months from April to October, 2003.

We checked validities of sp and z0 values adopted in the SST algorithm. Figure 5 depicts the SST difference between AMSR-E and buoy SSTs (the vertical axis) against 6H* (the horizontal axis), averaged from July to September 2003. If we were to specify appropriate values for both sp and z0, we would have a flat SST difference against 6H*. Six figures in Fig. 5 correspond to three SST ranges in the NH (right) and SH (left). The three SST ranges correspond to $2.5 < SST < 7.5$, $12.5 < SST < 17.5$, and $22.5 < SST < 27.5$°C. We calculated the mean values if the sample number for averaging exceeds 10. The standard deviations from the mean values range between 0.8 and 1.3°C for SST5°C, between 0.5 and 1.0°C

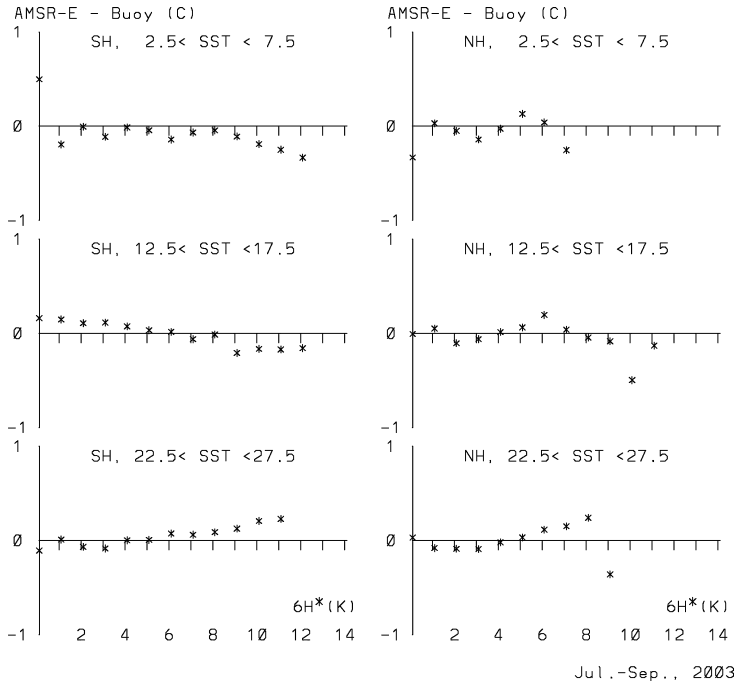

Fig. 5. SST difference between AMSR-E and buoy (°C) against 6H*, averaged during three months from Jul. to Sep. 2003 for three SST ranges in NH (right) and SH (left).

for SST15°C, and between 0.5 and 0.7°C for SST25°C. Figure 5 reveals that the SST difference was almost flat compared to 6H*, and indicates that the sp and z0 values were appropriately specified.

5. Extreme Cases

We reported an anomalous microwave emission in the Arabian Sea in summer, which we detected using the 10 GHz data of the TRMM Microwave Imager (TMI) aboard the Tropical Rainfall Measuring Mission (TRMM) (Shibata, 2003). We can now recheck it using the AMSR 6 GHz and SeaWinds data. The cause of the anomalous emission was considered to be a positive difference between the air and sea temperatures under strong wind conditions. In contrast, a negative difference between air and sea temperatures might induce another anomalous emission. We shall examine the Western Atlantic Ocean in winter using AMSR-E data, since we have no AMSR data in winter.

5.1 Arabian Sea in summer

Similarly to the TMI SST, we investigated the AMSR SST in the Arabian Sea in summer. Figure 6(a) depicts the monthly average of the SST difference between the AMSR and Reynolds in July 2003 in the Arabian Sea. We took the daily AMSR SST and subtracted the Reynolds SST on a corresponding day from AMSR, where the daily Reynolds SST was interpolated from the Reynolds weekly SST. We noticed a negative difference of SST along the coast of the Arabian Peninsula.

Figure 6(b) illustrates the monthly average of the difference between the air temperature and Reynolds SST in July 2003. The air temperature was adopted from the weather forecast model of the Japan Meteorological Agency (JMA), known as the Global Analysis (GANAL). The spatial resolution of the GANAL is 1.25 degree in both longitude and latitude directions. The time interval of the GANAL is 6 hour, i.e., 4 data points per day. We averaged the 4 data sets each day, and interpolated them spatially into 0.25-degree interval grids. The measurement height of air temperature is 2 m above the sea surface.

We noticed a positive air-sea temperature difference in the Arabian Sea, particularly in the Gulf of Aden. Table 2 shows a time sequence of the air-sea temperature in an area defined by A (longitudes between 42° and 55°E and latitudes between 10° and 20°N). The air-sea temperature difference was negative or slightly positive between April and mid-June 2003. It became positive in both July and August 2003. It decayed from late August to September and it became negative again in October 2003.

Figure 7 depicts the relations of 6V* and 6H* in the area A of the Arabian Sea in several months in 2003 (upper left: May 1–31, upper right: July 1–31, lower left: August 1–31, and lower right: September 21–October 20). The air-sea temperature difference was slightly positive in May. No strong winds blew in May, and the relation

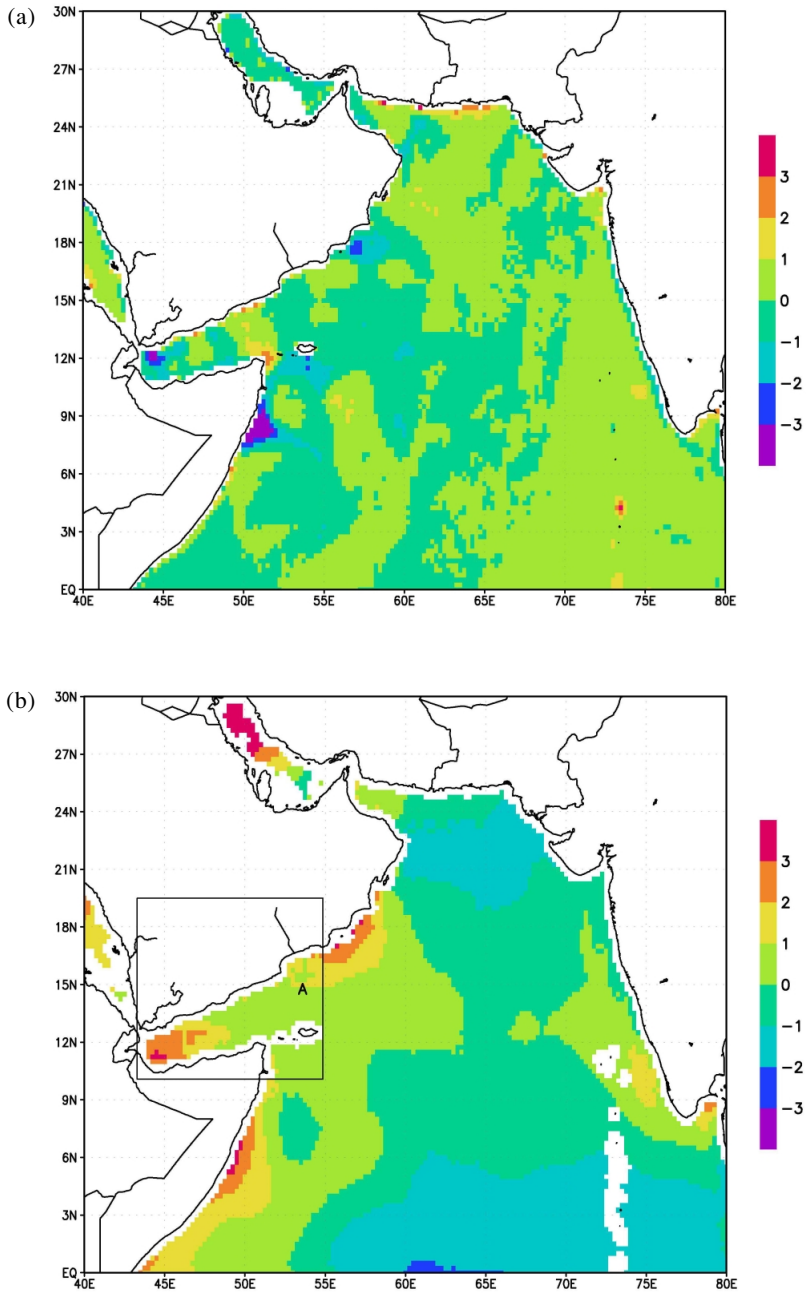

Fig. 6. (a) SST difference between AMSR and Reynolds (°C) in the Arabian Sea in Jul. 2003, (b) air-sea temperature difference in the Arabian Sea in Jul. 2003.

between 6V* and 6H* is not clear. The air-sea temperature was positive in July. The relation under crosswind condition in July was very different from that in the global ocean shown in Fig. 2(a), i.e., 6V* does not change until around 9 K of 6H*, and it then increases with 6H*. The slope of 6V*/6H* above 9 K is similar to that in the global ocean. The relation under downwind conditions in July also appears to differ from the global ocean, i.e., it does not change until around 6 K of 6H*. The relation under upwind conditions was similar to the global ocean. The situation in August was similar to July. In the period from late September to mid-October, the air-sea temperature difference was slightly positive or negative. The relation of 6V* and 6H* in this period was almost the same as the global ocean in Fig. 2(a). The value of inc_6V calculated by Eq. (3) exceeded the value necessary for wind correction under both crosswind and downwind conditions in July and August, and AMSR SST was less than

Table 2. Air-sea temperature difference averaged in the area A from April to October 2003. Three values in each month correspond to 10-day averages; the first, middle, and last month.

Apr.	May	Jun.	Jul.	Aug.	Sep.	Oct.
–0.4/0.2/–0.1	0.0/0.4/0.1	–0.1/0.4/0.8	1.2/1.1/0.9	0.9/1.1/0.9	0.6/0.6/0.1	–0.7/–0.7/–0.8

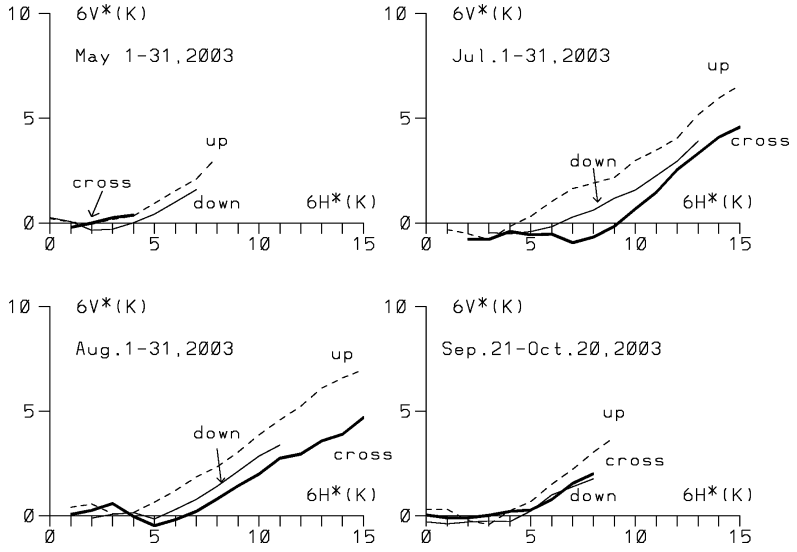

Fig. 7. Relations of 6V* and 6H* in the Arabian Sea in several months.

the correct value.

We compare 6V(H)* with the SeaWinds wind speed in July 2003 in Fig. 8 (upper: 6V*, lower: 6H*). The solid line corresponds to the area A and the thin line to the global ocean, both for the crosswind direction. The average SST in the area A in July 2003 was 27.1°C and the SST in the global ocean case was restricted to between 26 and 28°C. 6V* in the area A differed significantly from the global ocean, and 6H* was also slightly different from the global ocean, when the SeaWinds wind speed exceeded 7 m/s.

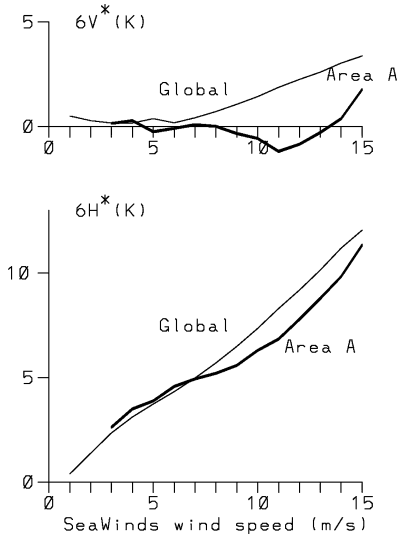

Fig. 8. Comparison of 6V* and 6H* relations between the area A in the Arabian Sea (solid line) and global ocean (thin line) in Jul. 2003.

5.2 Western Atlantic Ocean in winter

The air-sea temperature difference became negative in both the Western Atlantic and Western Pacific Ocean in winter. Figure 9 illustrates the air-sea temperature difference averaged between January and March 2003. The method used to generate Fig. 9 was the same as that for Fig. 6(b). The figure reveals a region with substantial negative values (an unstable region) in the Northern Western Atlantic Ocean. The air-sea temperature difference was slightly negative or neutral in other regions (neutral regions).

Figure 10 depicts the SST difference (°C) between the AMSR-E and buoy in two regions (B and C shown in

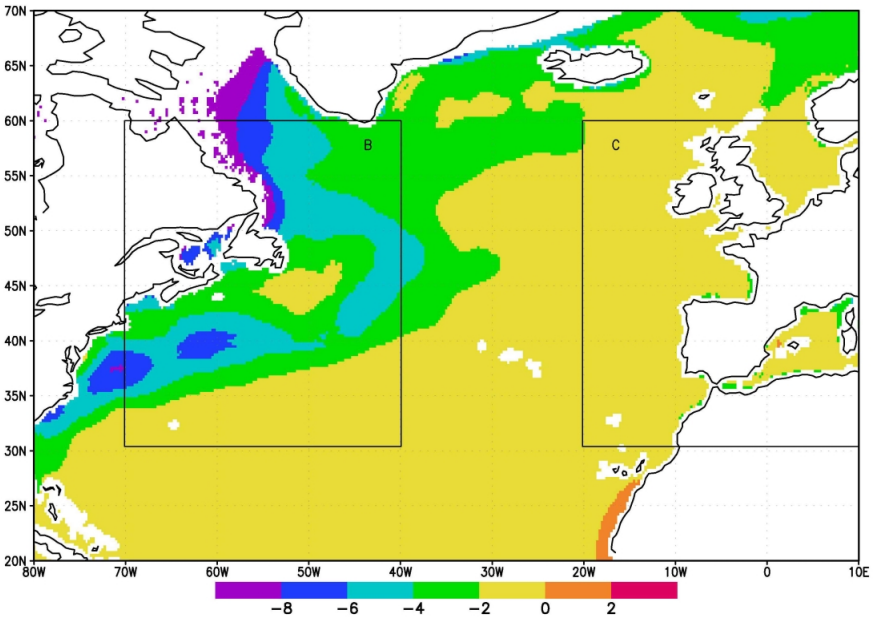

Fig. 9. Air-sea temperature difference (°C) in the Atlantic Ocean averaged from Jan. to Mar. 2003.

Fig. 9) between January and March 2003. Region B corresponds to longitudes between 70° and 40°W and latitudes between 30° and 60°N, and region C to longitudes between 20°W and 10°E and latitudes between 30° and 60°N. Region B is correlated with an unstable region and region C with a neutral region. We calculated the SST difference, when more than ten matched samples existed in any 1 K interval of 6H*. We noticed a positive SST error above 4 K of 6H* in region B. We could find no SST error in region C.

The results in Fig. 10 indicate that the sp values in region B differed from those in the global ocean. We could obtain the correct SSTs here, if we simply increase the sp from the global value.

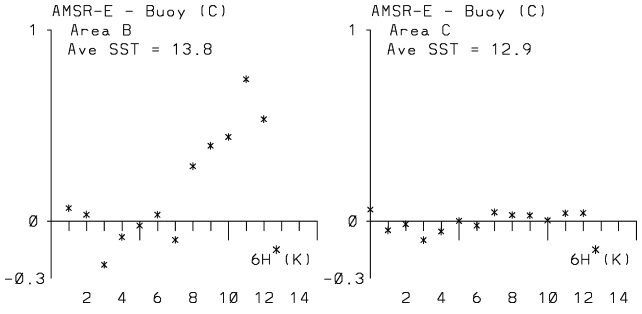

Fig. 10. SST difference (°C) between AMSR-E and buoy averaged from Jan. to Mar. 2003, against 6H*. Left figure is from the area B, and right figure is from C.

6. Conclusions and Discussions

Ocean microwave emissions changed by the ocean wind at 6 GHz have been investigated by combining data of the AMSR and SeaWinds aboard ADEOS-II. The relations of 6V* and 6H* were investigated first by using data from the global ocean in July 2003, which indicated that the relations of 6V* and 6H* vary with relative wind directions and with SSTs. These relations were then investigated separately in the NH and SH and also among different months, which revealed that the relations vary between the NH and SH and among months. These results indicate that we should specify the sp value for SST between the NH and SH, and among months. We obtained the correct SSTs with no cross-talk from 6H* by appropriately specifying the sp value.

We observed two extreme cases that differed from the global data; these regions were the Arabian Sea in summer, and the Western Atlantic Ocean in winter. The air-sea temperature difference was largely positive in the Arabian Sea in summer, and 6V* and 6H* relations differed from the global ocean with cross- and downwind directions. AMSR's SST became less than the correct value in this area. The air-sea temperature difference was largely negative in the Western Atlantic Ocean in winter, and the sp in this area might become greater than the global ocean. In that event, AMSR-E's SST exceeded the correct value. The current JAXA SST algorithm is not adapted to these extreme cases.

This paper has not discussed the physical mechanism that explains the microwave emissions changed by the ocean wind. We briefly discuss this mechanism now, leaving the details to future work. Foam and whitecaps over the ocean under strong wind conditions change the microwave emission. The generating mechanism of foam and whitecaps may depend on stability between the air and sea conditions. Parameters defining the stability may be listed as SST, air-sea temperature difference, swells, winds, and so on. The density of foam and whitecaps may vary with either swell slope facing the up- or down-wind directions. Furthermore, the shape of foam and whitecaps might change with either swell slope. The AMSRs view this foam and whitecaps. The complex relative dielectric constant of foam and whitecaps might change slightly between the V-pol and H-pol. Several results reported in this paper, such as different behavior at the SST30°C, different behavior between the northern and southern hemisphere, *et al.*, might be related to the complicated behavior of foam and whitecaps.

For a future SST algorithm, studies of parameterizations of the sp should be conducted, using an appropriate physical model. Such studies may enable us to calculate sp in individual cases by specifying the oceanic and atmospheric conditions, instead of specifying the sp values seasonally in two hemispheres with the current algorithm.

Acknowledgements

This work was supported by the ADEOS-II project with JAXA EORC. I am grateful to the Jet Propulsion Laboratory for providing us with the SeaWinds data. I am also grateful to Makoto Yoshikawa of the Mitsubishi Space Software Co. for handling the SeaWinds data, and to Taro Mutoh and Tomohiro Katoh of the Remote Sensing Technology Center of Japan for creating the collocated buoy data set.

References

Hollinger, J. P. and R. C. Lo (1984): Determination of sea surface temperature with N-ROSS. Naval Research Laboratory Memorandum Report 5375.

Kawanishi, T. *et al*. (2003): The Advanced Microwave Scanning Radiometer for the Earth Observing System (AMSR-E), NASDA's contribution to the EOS for Global Energy and Water Cycle Studies. *IEEE Trans. Geosci. Remote Sensing*, **41**, 184–194.

Klein, L. A. and C. T. Swift (1977): An improved model for the dielectric constant of sea water at microwave frequencies. *IEEE Trans. Antennas and Propagation*, **25**, 104–111.

Liu, W. T. (2002): Progress in scatterometer application. *J. Oceanogr*., **58**, 121–136.

Reynolds, R. W. and T. M. Smith (1994): Improved global sea surface temperature analyses. *J. Climate*, **7**, 929–948.

Shibata, A. (2003): A change of microwave radiation from the ocean surface induced by air-sea temperature difference. *Radio Science*, **38**(4), 8063–8072.

Shibata, A. (2004): AMSR/AMSR-E SST algorithm developments: removal of ocean wind effect. *Italian J. Remote Sensing*, **30/31**, 131–142.

Wentz, F. J. (1992): Measurements of oceanic wind vector using satellite microwave radiometers. *IEEE Trans. Geosci. Remote Sensing*, **30**, 960–972.